DOI 10.1007/s11141-024-10322-x
Radiophysics and Quantum Electronics, Vol. 66, Nos. 7–8, December, 2023
(Russian Original Vol. 66, Nos. 7–8, July–August, 2023)

COMPARISON OF MILLIMETER RADIO INTERFEROMETRY METHODS FOR FAST PROCESSES WITH AND WITHOUT FREQUENCY CONVERSION

V. V. Balandin,[1] **Vl. Vl. Balandin,**[1]
A. V. Vodopyanov,[1,2] **D. A. Mansfeld,**[1,2]
K. V. Mineev,[1,2] * **V. V. Parkhachev,**[1] **and**
R. M. Rozental [1,2]

UDC 662.331+621.3.029.65

We compare two methods of millimeter radio interferometry with and without frequency conversion using as an example experimental measurements of the transverse deformation magnitude of a metal rod under dynamic load. We reveal a good agreement between the results, demonstrating a possibility of measuring the surface deviations within times of about 1 μs with micron precision.

1. INTRODUCTION

Currently, millimeter-wavelength radio interferometers are widely used for non-contact diagnostics of shock wave and detonation processes [1–4], studying impacts of objects with obstacles [5], measuring the dynamic Poisson coefficient of materials [6], studying the characteristics of shock-compressed plasma [7, 8], and measuring the burning rate for materials [9, 10]. Compared with laser methods, the microwave diagnostics has certain advantages for some special tasks since the wavelengths of the probing radiation differ by several orders of magnitude so that there are qualitative differences in the capabilities of the methods, and significantly different hardware equipment is required. The characteristic sizes of irregularities reflecting microwave radiation, e.g., of the ones associated with inhomogeneities of the detonation fronts or surface roughness of striker and shell, are significantly smaller than the radiation wavelength. Therefore, such surfaces for microwave radiation are almost smooth, whereas they are diffusely reflective for laser radiation, and the diffuse reflector creates certain difficulties in diagnosing and deciphering the results.

To date, there are commercially available and metrologically certified radio interferometers capable of measuring the displacement of moving reflective surfaces with an error below $0.1-0.2$ mm [11]. The high sensitivity of the microwave method to the motion of various interfaces, the possibility of conducting research in optically opaque dielectrics, and the continuity of obtained data provide ample opportunities in experimental studies. The advantages of non-invasive microwave diagnostics over traditional contact research methods allow one to obtain fundamentally new information about the processes occurring in substances exposed to intense dynamic loads in some cases [12].

As in laser interferometry (the Michelson scheme), the Doppler effect underlies the operation principle of microwave radio interferometers. In a typical radioelectronic "reflection interferometer" [13], the oscillation phases of the reference microwave signal and the signal reflected from the object observed are compared. When the position of the object is changed, a proportional phase shift of the reflected signal arises; the

* mineevkv@gmail.com

[1] N. I. Lobachevsky State University of Nizhny Novgorod; [2] A. V. Gaponov-Grekhov Institute of Applied Physics of the Russian Academy of Sciences, Nizhny Novgorod, Russia. Translated from Izvestiya Vysshikh Uchebnykh Zavedenii, Radiofizika, Vol. 66, Nos. 7–8, pp. 697–706, July–August 2023. Russian DOI: 10.52452/00213462_2023_66_07_697 Original article submitted April 25, 2023; accepted June 19, 2023.

surface displacement magnitude magnitude can be restored from this shift. In the future, one can calculate the velocity and movement of a reflecting surface based on this information.

However, this apparently simple operation principle requires the construction of a rather complex measurement scheme in the millimeter wavelength range. Commonly, the receiving radio interferometer device uses the frequency conversion and the subsequent quadrature demodulation of the output interference signals. Because of the overlap between the spectra of the useful signal and of various low-frequency noises of the homodyne receiver, a superheterodyne scheme with intermediate frequencies of the reference and receiving (information) channels within a range of a few gigahertz is used in radio interferometers more often. The development of digital recording methods allowed the digital signal processing at the intermediate frequency directly without analog units of the quadrature phase detection.

At the same time, the upper values of the operation frequencies of digital oscilloscopes offered by the world's leading manufacturers currently allow direct recording of the millimeter-range signals with frequencies up to 110 GHz, and a further extension of this range is only a matter of time with the rapid development of the next generations of wireless communication systems [14]. Therefore, the scheme of radio interferometric measurements can be significantly simplified. Now it can contain a stable high-frequency oscillator, a transceiving waveguide path, and a high-speed digital oscilloscope only. Similar schemes have already shown their best when measuring the plasma-process parameters [15, 16].

Using an example of measuring the transverse widening of a metal rod under the action of a longitudinal compression pulse, this work compares two radio interferometric measurement schemes, namely, a classical one with frequency conversion and a one without frequency conversion, as an example. The experiment was carried out at Research Institute for Mechanics of Lobachevsky State University of Nizhny Novgorod.

2. EXPERIMENTAL SETUP

Experimental studies used the RSG-60 setup, which implements the classical version of Kolsky compression method [17]. This setup consists of an exciting device, which is a 57 mm gas gun where compressed air is used to accelerate the striker, and two measuring rods 1.5 m long each. Only one measuring rod was used during the experiments with radio interferometers. The D16T-alloy rod with a diameter of 60 mm and a length of 1.5 m excited by an impact of a striker made of the same alloy and accelerated to the required striker velocity V was used as a measurement object (see Fig. 1). In the experiments, the impact velocity was chosen to avoid plastic strain of the rod and amounted to about 10 m/s. A longitudinal elastic wave of compressive stresses propagating along the rod [19] is known to emerge as a result of longitudinal elastic impact and the absence of geometric dispersion [18] in a thin rod whose transverse dimensions are small compared with its length. The duration of the elastic pulse in a rod is determined by the doubled length of the exciting striker and the sound velocity in the rod. The stress-strain state of the rod material is uniform over the transverse cross sections. The longitudinal compressive deformations of the rod material are accompanied by transverse tensile deformations. The ratio of the respective transverse and longitudinal deformations is equal to the Poisson ratio.

The longitudinal elastic compressive deformation of the rod was determined from the signals recorded from short-base resistive strain gauges glued onto the rod surfaces in the cross section at a distance of the rod half-length from the impacted end. In turn, the magnitude of the transverse deformation was determined based on the interferometry data.

The transceiving antenna systems of two radio interferometers of the W-band (with frequency conversion) and K_a band (without frequency conversion) were located near the rod. The deformation wave traveling along the rod at the sound velocity c caused similar changes in the rod diameter at both measurement points with a time delay proportional to the distance L between the antenna systems. The antenna systems were located at the angles α_1 and α_2 with respect to the normal to the rod surface.

One transceiving channel of the RI-03/3 [3] W-band multichannel radio interferometer with its key-unit structural layout is shown in Fig. 2 was used for the frequency-conversion measurements. The main

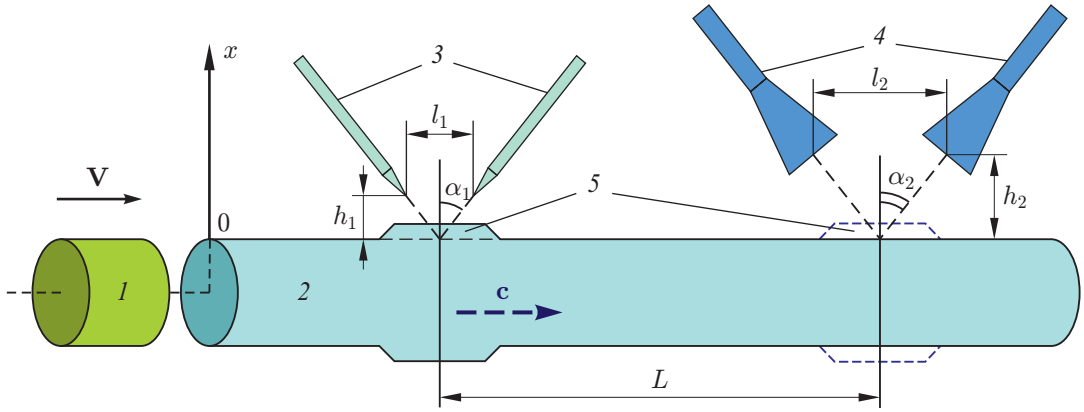

Fig. 1. Experimental setup: striker *1*, metal rod *2*, antenna systems of the interferometers) *3* and *4*, respectively, of the W band (with frequency conversion), and K_a band (without frequency conversion, and transverse deformation wave *5*.

RI-03/3 radio interferometer unit, which is marked by the dashed line in Fig. 2, is a coherent transceiver synchronized by a stable signal with the frequency $f_{\text{ref}} = 100$ MHz from quartz oscillator *1*. The signal is divided into two channels using divider *2* and is delivered to the high-frequency oscillators. In each channel, the signal at the frequency f_{ref} serves as a reference one for the phase-lock loop frequency control system of the centimeter-wavelength synthesizers within dielectric resonators. These synthesizers are used in oscillators *3* and receiver *4* of transmitter and receiver heterodyne, respectively. The main operating frequencies of the transmitter ($f_0 = 93.7$ GHz) and heterodyne ($f_{\text{H}} = 91.7$ GHz) signals result from the upconversion of the centimeter-range frequency (to millimeter range) by the high-order harmonic multipliers based on avalanche diodes and the subsequent narrow-band filtering and amplification to the operation levels. The outputs of the high-frequency oscillators *3* and *4* are the rectangular metal waveguides of conventional cross section 2.4×1.2 mm. Using a directional coupler *5*, a small part of the signal in the transmitting path is delivered to the balance mixer *6*, whereas the main power is used for the object probing. Ferrite gate *7* is installed in the output path so that the reflected radiation is suppressed. Radiation between the radio interferometer and the measured object was transported using rectangular dielectric waveguides with a length of about 3 m and a cross section of 1×2 mm (losses per unit length amounted to about 2.5 dB/m in the W range). Matching between the metal and dielectric waveguides is done using smooth transition *8* [20]. Open ends of dielectric waveguides with a 7 mm long tapering were used as an antenna system *9* (the main lobe width of the radiation pattern at the level -3 dB is $\Theta_{-3\,\text{dB}} = 45°$).

The heterodyne signal was divided between the balance mixers *6* and *10* of the transmitter and the receiver, respectively, by divider *11* installed on the waveguide ring junction. Thus, the signals at the intermediate frequency

$$f_{\text{i}} = f_0 - f_{\text{H}} \tag{1}$$

are isolated at the outputs of the balance mixers of the transmitter and receiver with the only difference that the received signal which is reflected from the studied object has an additional phase incursion.

The signal at the intermediate frequency was recorded by digital oscilloscope *12* with operation band of 2.5 GHz and a discretization frequency of 10^{10} s^{-1}.

The diagram of the K_a-band interferometer operating without frequency conversion is given in Fig. 3. The 6 high-frequency Gunn-diode oscillator G4-15 *1* used in this scheme delivers the signal at the frequency $f_0 = 32.5$ GHz. A part of the signal from the oscillator was separated using the 10-dB waveguide directional coupler *2* and was delivered to the input of digital oscilloscope *4* via waveguide-coaxial transition *3*. Ferrite gate *5* was installed in the output path for suppressing reflected radiation. The transceiving antenna system *6* comprised two metal pyramidal flares with an aperture of 20×20 mm ($\Theta_{-3\,\text{dB}} = 30°$).

The signal reflected from the object and received by the antenna was also delivered to the oscilloscope

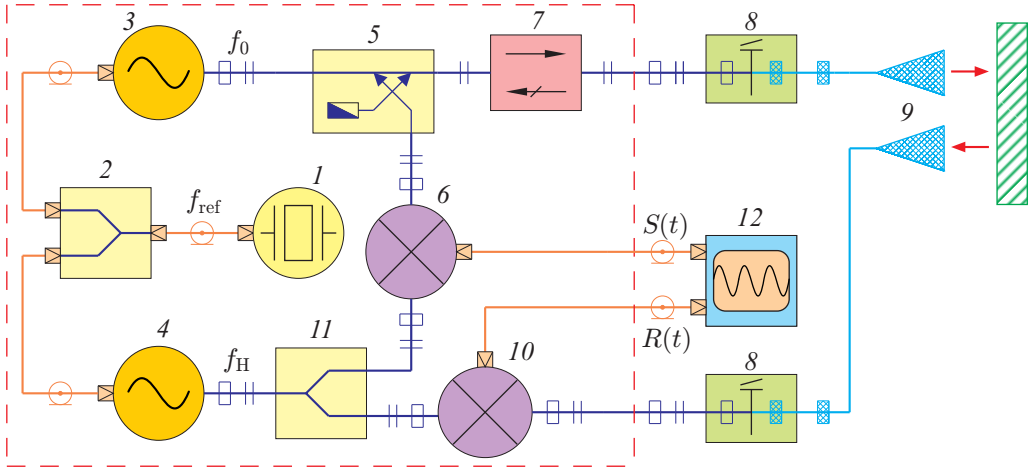

Fig. 2. Block diagram of the W-band interferometer with the frequency conversion: quartz oscillator *1*, power divider *2*, high-frequency oscillators *3* and *4* of transmitter and heterodyne signals, respectively, waveguide directional coupler *5*, balance mixer *6* of the reference channel, ferrite gate *7*, transition *8* between dielectric and metal waveguides, antenna system *9*, balance mixer *10* of the receiving channel, power divider *11*, and digital oscilloscope *12*. The dashed rectangle indicates the main unit of the RI-03/3 radio interferometer.

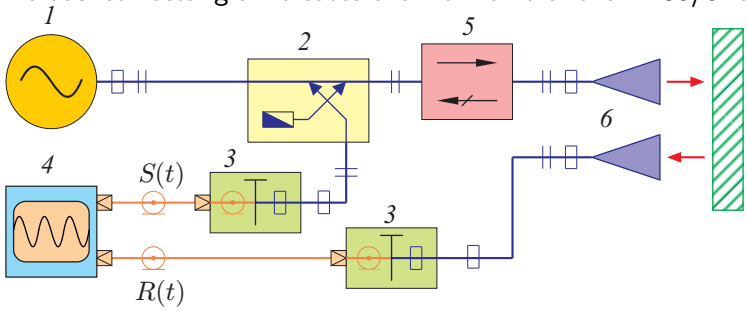

Fig. 3. Block diagram of the K_a-band interferometer without the frequency conversion: high-frequency oscillator *1*, waveguide directional coupler *2*, waveguide–coaxial transition *3*, digital oscilloscope *4*, ferrite gate *5*, and antenna system *6*.

input via the waveguide–coaxial transition. The signals were recorded using a digital oscilloscope with a transmission band of 59 GHz and a discretization frequency of $1.6 \cdot 10^{11}$ s^{-1}.

All antennas were oriented along the horizontal plane containing the axis of the metal rod. In the absence of the reflecting surface, discrimination between the receiving and transmitting channels of the radio interferometers was at least −30 dB.

3. PROCESSING AND ANALYSIS OF RESULTS

The following signal processing algorithm was used in the case of interferometry in the W band with frequency conversion. Let the reference signal have the form

$$S(t) = A_0 \cos(\omega t + \varphi_0), \tag{2}$$

where $\omega = 2\pi f_{\text{i}}$, A_0 and φ_0 are the initial amplitude and phase of the signal, respectively, and f_{i} is the intermediate frequency. In turn, the received (information) signal has the form

$$R(t) = A_1 \cos[\omega t + \varphi_0 - \Delta\varphi(t)], \tag{3}$$

where A_1 is the amplitude of the received signal and $\Delta isthe\varphi(t)$ is the additional phase incursion.

An additional phase incursion contains the invariable part φ_1, which is determined by the initial distance to the studied object and the reflection conditions from it, and the variable part determined by a variation in the distance to the object during the experiment,

$$\Delta\varphi(t) = \varphi_1 + kL(t), \tag{4}$$

where $k = 2\pi/\lambda$ is the wave number and $L(t)$ is the variation in the path length covered by the probing signal. If we take into account that the probing angle was $\alpha = \alpha_1$ (see Fig. 1) and the incident angle of the probing radiation is equal to its reflection angle, the variation $L(t)$ in the optical length of the path can be expressed in terms of the reflection-point displacement $x(t)$,

$$L(t) = 2x(t)\cos\alpha. \tag{5}$$

In the general case, the angle α varies with the object displacement. However, in the considered experiments, the displacement was only several micrometers, and the angle variation could be neglected.

Therefore, an additional phase incursion is

$$\Delta\varphi(t) = \varphi_1 + 2kx(t)\cos\alpha. \tag{6}$$

Since $\Delta\varphi(t) \ll \omega t$, the received signal is a narrowband one. To determine the instantaneous phase of the narrowband signals, it is convenient to use the formalism of the analytical signal which is a complex signal whose real part coincides with the initial signal, while the imaginary part is in the quadrature with the real part.

From practical viewpoint, the analytical signal can be most easily obtained through applying the frequency-band filter with the transmission coefficient $H(\omega) = 2\sigma(\omega)$ to the initial end signal where $\sigma(\omega)$ is the Heaviside function. After the filtering, the respective signals have the following form:

$$\hat{S}(t) = A_0 \exp\left[i\left(\omega t + \varphi_0\right)\right], \quad \hat{R}(t) = A_1 \exp\left[i\left(\omega t + \varphi_0 - \Delta\varphi(t)\right)\right]. \tag{7}$$

Useful information is contained in the phase difference $\Delta\varphi(t)$ of these signals. To avoid oscillations at the frequency ω and analyze only the meaningful time dependence, one should multiply the received signal by the signal that is complex conjugate to the reference signal. Then, the obtained signal, which is the process interferogram, can be expressed as [1, 21]

$$\hat{R}_{\text{int}}(t) = \hat{R}(t)\hat{S}^*(t) = A_0 A_1 \exp\left[-i\Delta\varphi(t)\right] = A\exp\left[i\Phi(t)\right], \tag{8}$$

where the superscript * denotes complex conjugation. Obviously, the interferogram is the complex envelope of the received signal with the additional factor A_0. A slow (on the scale $2\pi/\omega$) variation in the amplitude A_1 of the received signal if it is present, does not hinder retrieving information on the interferogram phase. The synchronous detection, which is used to obtain the interferogram, mitigates the influence of the phase noise in the probing oscillator.

The interferogram phase $\Phi(t)$ can be found as follows:

$$\Phi(t) = \arctan\frac{\text{Im}\left[\hat{R}_{\text{int}}\,(t)\right]}{\text{Re}\left[\hat{R}_{\text{int}}\,(t)\right]}. \tag{9}$$

It is noteworthy that the described procedure is optimal for estimating the phase of the narrowband signal against the background of Gaussian noise [22]. In turn, the displacement of the reflecting boundary of the studied object is found from the following relation:

$$\frac{\Phi(t)}{2k\cos\alpha} = -\frac{\Delta\varphi(t)}{2k\cos\alpha} = -\frac{\varphi_1 + 2kx(t)\cos\alpha}{2k\cos\alpha} = -x(t) - \frac{\varphi_1}{2k\cos\alpha}. \tag{10}$$

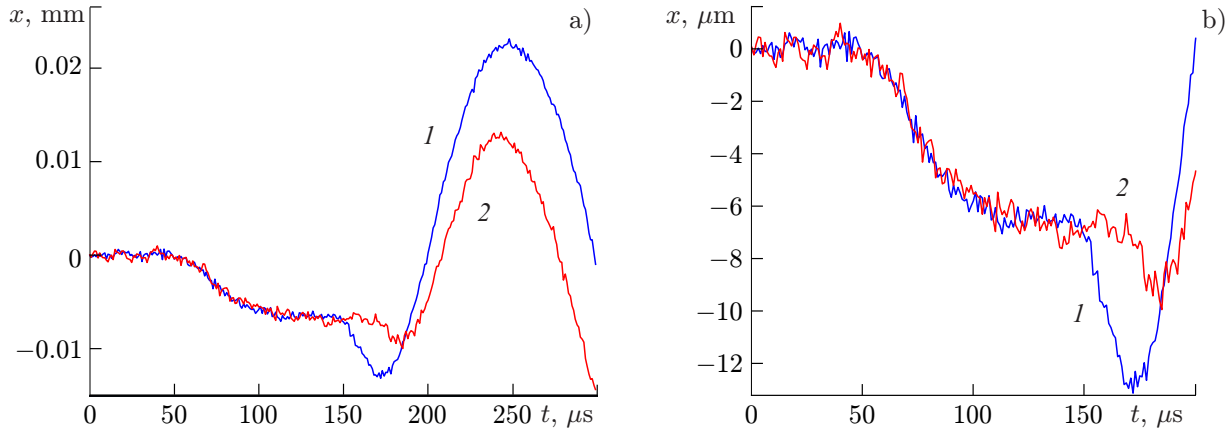

Fig. 4. The dependences of the displacement x of the rod surface on the time t in two different time scales (*a* and *b*). Curves *1* and *2* correspond to the measurements with and without the frequency conversion, respectively.

Assuming that the displacement at the initial time instant is equal to zero, i.e., $x(0) = 0$, we find the unknown constant $\varphi_1 = -\Phi(0)$ and, as a result, we obtain

$$x(t) = \frac{\Phi(0) - \Phi(t)}{2k\cos\alpha}. \tag{11}$$

In the interferometry scheme in the K_a band without frequency conversion the signal processing was done in a similar manner. However, in this case, the value of $\omega = 2\pi f_0$ was determined by the frequency of the probing signal rather than the by intermediate frequency.

Irrespectively of the interferometry scheme used, the estimation accuracy of the displacement can be improved if the values of $x(t)$ are averaged over a certain sufficiently short time interval, over which the variation in the coordinate of the studied object can be neglected. However, at high noise levels, there might appear an unavoidable removable modulo-2π ambiguity in determining the instantaneous phase of the interferogram and, therefore, we should average (complex) values of the interferogram $\hat{R}_{\text{int}}(t)$ rather than the phase or displacement over a certain time interval and then determine the phase of the averaged interferogram. In our experiments, the averaging was done over a time interval of 1 μs.

An experimental series of ten experiments was carried out. The time dependences of displacement (movement), which were obtained from the measurements in the W band with the frequency conversion (curves *1*) and in the K_a band without frequency conversion (curves *2*) are shown in Fig. 4 for the experiment in two scales (Figs. 4*a* and 4*b*).

Although a deformation wave passes by the probed regions of two interferometers at different times since there is a shift between the interferometers (see Fig. 1), so curves *1* and *2* in Fig. 4 are shifted in time to ensure convenient comparison. The transverse strain wave measured is observed starting from the time 50 μs and has a duration of about 100 μs. A bending wave emerging in the rod because of the imperfect axial symmetry of the impact is detected from the time instant 150 μs, which corresponds to a sharp change in the character of the displacement dependence. Since the bending wave has a lower velocity compared with that of the compression wave, it arrives with a delay. Since there is a shift between the antenna systems of two interferometers, the bending wave recorded by them has different phases, and curves *1* and *2* do not coincide after its arrival.

Figure 4 clearly shows that both interferometers demonstrate almost the same displacement dependences on time before arrival of the bending wave. The value spread of the displacement-estimation noise component characterizing the measurement accuracy is in both cases at the level ± 1 μm, which is confirmed by the plots in Fig. 5. These dependences were obtained from the test signal which was recorded from the

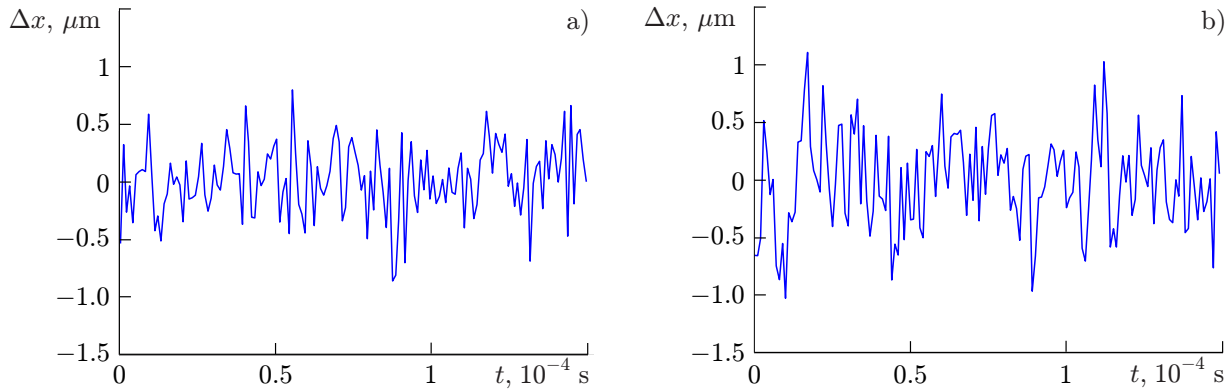

Fig. 5. The dependences of the spread Δx of the measurement results for the motionless surface on time t: (a) the measurements with the frequency conversion (in the W band) and (b) without the frequency conversion (in the K_a band).

motionless rod immediately before the experiment.

The results obtained for displacement estimation from two interferometers differed by no more than 1 μm for all experiments in the series, i.e., the measurement results from two devices coincided within the error limits of each interferometer.

The distance L between the antenna systems in Fig. 1 was 200 mm while the difference in the signal-arrival times was about 40 μs. This data was used to determine the velocity of the strain wave propagation along the rod amounting to $c \approx 5000$ m/s in the performed experiments, which differed by less than 2% from the reference value 5080 m/s for the sound velocity in the material used [23].

The Poisson ratio ν of the rod material can be found as a ratio of the transverse ε_2 deformation to the longitudinal ε_1 one,

$$\nu = -\varepsilon_2/\varepsilon_1. \tag{12}$$

As was mentioned above, the longitudinal deformation ε_1 in our experimental series was measured by the resistive strain gauges. For all experiments in the series, the Poisson-ratio estimate was within the interval 0.33–0.37. According to the data [23, 24], the Poisson ratio of alloy D16T amounts to 0.32–0.33. The obtained estimates partially overlay with the above interval, and the greatest deviation of our estimates from the upper boundary of the interval amounts to 10%. The differences can be due to the presence of the bending wave, which prevents us from correct estimation of the rod widening. To improve the measurement accuracy, one can probe the sample from two sides [6]. Inaccuracies in determining the location angles of the antenna systems can be another cause of the estimation error for the Poisson ratio. This problem might be solved by precise stencils that level the antennas on the test bench.

4. CONCLUSIONS

We have experimentally demonstrated a possibility of measuring the amplitude of impact-excited transverse deformations of a metal rod. The measurements were performed using the millimeter radio interferometers of two types: with and without frequency conversion in the W and the K_a bands, respectively. Coincidence of the results of two independent measurements within the same experiment testifies to the potential reached accuracy of ± 1 μm over time interval of 1 μs.

The capabilities of modern measuring technology make it possible to use various schemes for constructing high-frequency paths of radio interferometers, including those without frequency conversion, such that the measurement accuracy does not decrease. However, it is extremely important to use a stable signal generator with a low level of phase noise as well as a digital recorder which has not only a wide operating bandwidth and a high sampling rate but also a sufficient amount of memory per channel to be able to register the entire signal of the process under study. However, in the case of continuous monitoring of slow processes,

hardware isolation of the complex envelope of the received signal may still be preferable. It is worth noting that when a radio interferometer with frequency conversion is used, the output signal at the intermediate frequency can be easily amplified by a low-noise amplifier with the subsequent discussion for both direct registration of the intermediate frequency by the digital oscilloscope and hardware quadrature-phase detection where the most informative parts of the process are recorded at the given frequency, while the entire process is recorded in the main frequency band. In the case of using a radio interferometer without frequency conversion, to record a slow process, one should switch the digital oscilloscope to the segmented-recording mode with synchronization of the start from an external gate signal or an internal timer.

This work was supported by the Russian Science Foundation (project No. 21-19-00283).

REFERENCES

1. V. M. Bel'skii, A. L. Mikhailov, A. V. Rodionov, and A. A. Sedov, *Combust. Expl. Shock Waves*, **47**, No. 6, 639–650 (2011). https://doi org/10.1134/S0010508211060037
2. E. V. Botov, V. N. Ikonnikov, V. A. Kanakov, et al., *Radiophys. Quantum Electron.*, **61**, No. 5, 382–388 (2018). https://doi. org/10.1007/s11141-018-9899-y
3. V. A. Kanakov, S. V. Katin, N. S. Kornev, et al., *Antennas*, No. 1, 49–54 (2016).
4. R. O. Mays, J. W. Tringe, P. C. Souers, et al., *AIP Conf. Proc. 1979*, 160016 (2018). https://doi.org/10.1063/1.5045015
5. V. V. Balandin, Vl. Vl. Balandin, V. V. Parkhachev, and D. A. Lamzin, *Problems of Strength and Plasticity*, **80**, No. 1, 118–126 (2018). https://doi.org/10.32326/1814-9146-2018-80-1-118-126
6. V. V. Balandin, Vl. Vl. Balandin, A. K. Lomunov, and V. V. Parkhachev, *Problems of Strength and Plasticity*, **82**, No. 4, 413–427 (2020). https://doi.org/10.32326/1814-9146-2020-82-4-413-427
7. V. A. Ogorodnikov, A. L. Mikhailov, V. V. Peshkov, et al., *J. Exp. Theor. Phys.*, **114**, No. 1, 161–166 (2012). https://doi.org/101134/S106377611115012X
8. E. N. Bogdanov, M. V. Zhernokletov, G. A. Kozlov, and A. V. Rodionov, *Combust. Expl. Shock Waves*, **56**, No. 4, 479–485 (2020). https://doi.org/10.1134/S0010508220040127
9. V. E. Zarko, D. V. Vdovin, and V. V. Perov, *Combust. Expl. Shock Waves*, **36**, No. 1, 62–71 (2000). https//doi. org/10.1007/BF027001515
10. A. S. Zharkov, M. G. Potapov, V. P. Lushev, et al., *Combust. Expl. Shock Waves*, **36**, No. 1, 72–75 (2000). https//doi. org/10.1007/BF02701516
11. A. V. Kashin, N. S. Kornev, K. V. Mineev, et al., *Proceedings of the 8th International Scientific Conference on Military Technical Problems. Defense and Safety. Application of Dual-Use Techniques, May 16–17, 2019, Minsk, Belarus* [in Russian], Vol. 4, pp. 21–24.
12. A. L. Mikhailov, ed., *Nonperturbing Methods for Diagnostics of Fast-Running Processes* [in Russian], Federal State Unitary Enterprise "Russian Federal Nuclear Center All-Russia Science and Research Institute of Experimental Physics," Sarov (2015).
13. N. A. Zlatin, ed., *Physics of High-Speed Processes* [in Russian], Vol. 1," Mir, Moscow (1971).
14. T. S. Rappaport, Y. Xing O. Kanhere, et al., *IEEE Access*, **7**, 78729–78757 (2019). https://doi.org/10.1109/ACCESS.2019.2921522
15. R. A. Kornev, P. G. Sennikov, S. V. Sintsov, and A. V. Vodopyanov, *Plasma Chem. Plasma Process*, **37**, 1655–1661 (2017). https://doi.org/10.1007/s11090-017-9846-2
16. S. Sintsov, D. Mansfeld, E. Preobrazhensky, et al., *Plasma Chem. Plasma Process*, **42**, 1237–1247 (2022). https://doi.org/10.1007/s11090-022-10280-0

17. P. V. Demenko, *Problems of Strength and Plasticity*, **63**, 186–190 (2001).
18. H. Kolsky, *Stress Waves in Solids, Clarendon Press, Oxford* (1953).
19. V. N. Ionov and P. M. Ogibalov, *Stresses in Bodies under Pulsed Loading* [in Russian], Vysshaya Shkola, Moscow (1975).
20. V. F. Vzyatyshev, Yu. I. Orekhov, A. G. Pankratov, et al., RF Patent No. 2557472 (2006).
21. V. A. Kanakov, S. Yu. Lupov, Yu. I. Orekhov, and A. V. Rodionov, *Radiophys. Quantum Electron.*, **51**, No. 3, 210–221 (2008). https://doi.org/10.1007/s/1141-008-9021-y
22. B. R. Levin, *Theoretical Basis of Statistical Radio Engineering* [in Russian], Radio i Svyaz', Moscow (1989).
23. I. S. Grigor'ev and E. Z. Meilikhov, eds., *Physical Quantities: Handbook* [in Russian], Energoatomizdat, Moscow (1991).
24. A. L. Bardenshteín, V. I. Bykov, and D. I. Vaísburd, *JETP Lett.*, **61**, No. 2, 100–105.